Swirl Ratio and Post Injection Strategies to Improve Late Cycle Diffusion Combustion in a Light-Duty Diesel Engine

Authors:

Jesús Benajes[1], Jaime Martin[1], Antonio García[1], David Villalta[1], Alok Warey[2]

Affiliation:

1. CMT Motores Térmicos – Universitat Politècnica de València, Camino de Vera s/n, 46022, Valencia, Spain.
2. Propulsion Systems Research Lab, General Motors Global Research and Development.

Corresponding Author:

Dr. Antonio García

CMT - Motores Térmicos /Universitat Politècnica de València

angarma8@mot.upv.es

ABSTRACT

Nitrogen oxides (NOx) and soot emissions are the most important pollutants from direct-injection diesel engines. In particular, soot formation and oxidation determine the net engine-out soot emissions. These phenomena are complex and competing processes during diesel combustion. Despite many researches implicate the mechanisms of soot formation with soot emissions, the enhancement of the late cycle soot oxidation is the dominant mechanism for a reduction of engine-out soot emissions. The mixing process and the in-cylinder bulk temperature are two important parameters in the development of soot oxidation process. The current research compares different engine strategies to enhance the late cycle mixing controlled combustion process and therefore enhance soot oxidation while maintaining similar gross indicated efficiency in a light-duty engine. For this purpose, a simplified methodology has been used, which analyzes the effect of mixing process and in-cylinder bulk gas temperature on soot oxidation during the late cycle combustion. For carrying out this research, theoretical and experimental tools were used. In particular, the experimental measurements were made in a single-cylinder direct-injection light-duty diesel engine varying the swirl ratio and the injection pattern as injection pressure, Start of Energizing (SoE), Energizing Time (ET) and number of injections events. To analyze soot emissions, the combustion luminosity was measured by an optoelectronic probe and the optical thickness parameter (KL) was evaluated by the two-color pyrometry method. The apparent combustion time (ACT^{-1}) was used as mixing time tracer. Results show that an increase in swirl ratio implies an improvement on the mixing process and higher values of average bulk temperature during the late-cycle diffusion combustion. Both phenomena produce an enhancement in the soot oxidation process. In the lowest swirl ratio case, a suitable injection strategy based on multiple

injections, provides similar results of soot oxidation process (and therefore, the emissions) as high swirl ratio case.

1. INTRODUCTION

Due to the increase of Greenhouse Gas (GHG) emissions produced by the Internal Combustion Engines (ICE), stringent regulations are being introduced all around the world to limit their exhaust emissions with the objective of decreasing their environmental impact. The automotive manufacturers and researchers focus their attention on the development of cleaner and more efficient powertrain engines. In particular, the nitrogen oxides (NOx) and particulate matter (PM) are the most important pollutants from direct-injection diesel engines. Thus, different strategies are implemented to reduce these emissions: high pressure fuel injection systems [1, 2], multiple injections [3], high boost pressure [4], exhaust gases recirculation [5], high swirl [6], new cleaner fuels [7] and new combustion concepts [8, 9]. The present research was focused on comparing different engine operating conditions, which can achieve a reduction in engine-out exhaust emissions.

Soot emissions in diesel exhaust depend on formation and oxidation processes. Both processes are distinct in temporal and spatial evolution. The soot formation process is more important during the fuel injection event and it is approximatively located in the region closest to the nozzle [10]. Large amount of soot forms quickly during the earliest combustion period due to high local equivalence ratio in the fuel-rich premixed burn region [11, 12, 13]. In this stage, soot oxidation is poor. From the End of Injection (EoI), the soot oxidation process becomes more relevant. The oxidation stage spans the range from EoI up to the End of Combustion (EoC). In this stage, the diffusion flame disappears, the soot formation decreases and the soot oxidation rate increases. In these conditions, the mixing process and the in-cylinder bulk temperature govern the soot oxidation process. It is important to highlight that only a small amount of soot formed makes it into the exhaust. Figure 1 shows the correlation between the maximum amount of soot formed (peak value of soot concentration, KL) and concentration of PM emissions in the exhaust for different measured engine conditions [14]. Thus, two groups of results are clearly observed: on the one hand, the square symbols points out a group of results in which the PM emissions are similar and low independently on the peak value of soot concentration, KL and therefore independently on the value of soot formed in-cylinder. On the other hand, group of circle symbols indicate other results where the highest concentrations of soot formed, maximum of KL peak value correspond on lowest values of PM emissions, and vice versa. These trends are the opposite of those that would be expected if the PM emissions were explained by the amount of formed soot [15]. Gallo et al. have obtained a similar correlation. In their study [16], different operating conditions were measured in an optical engine and the laser extinction technique was used to evaluate the oxidation rates during the expansion stroke. They conclude that the amount of in-cylinder soot formed does not explain the engine-out soot emissions. Considering diesel fuel and operating conditions tested, the oxidation process is mainly responsible for the exhaust PM emissions in a CI diesel engine under real conditions.

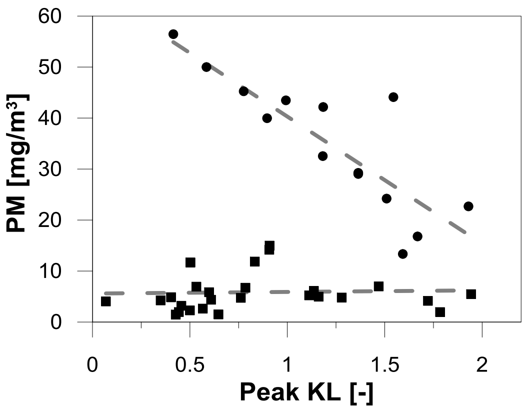

Figure 1. Concentration of exhaust PM versus the maximun value of KL for the diferent engine conditions measured in [14].

In literature, many researchers have studied the soot oxidation process. Dembinski et al. [17] studied the impact of swirl ratio and injection pressure on the soot oxidation process. Experimental measurements were made with two different optical techniques (Combustion Image Velocimetry and two-color method) in an optical engine. This research stated that the soot oxidation process improved when the swirl ratio and injection pressure were increased due to an enhancement of in-cylinder turbulence. O'Connor and Musculus [18] studied the effect of different engine parameters on the soot oxidation process, concluding that a post injection can reduce engine-out soot by up to 45% at high swirl ratios and 30% for low swirl ratios. Gallo et al. [16] analyzed the amount of PM emitted by modifying the injection pressure, gas density and temperature at TDC as well as engine speed and nozzle hole size by application of the laser extinction method. These authors concluded that increasing the injection pressure, gas density, and reducing nozzle hole size and the engine speed, the engine-out PM emissions were strongly reduced. Arrègle et al. [19] showed different post-injection strategies for reducing soot emissions in DI diesel engines. In this research, a broad experimental analysis was carried out to explore the behavior of post-injection strategy on exhaust soot emissions under a certain range of operating conditions and with different post-injection timings. These authors concluded that the engine-out soot emissions were reduced when the post-injection event was added. Using a similar optical approach, Lopez et al. [20] also studied the in-cylinder soot oxidation process by means of the two-color method. In particular, the impact of swirl, EGR and injection timing were analyzed. These authors concluded that the soot oxidation process is degraded when swirl is decreased, EGR rate is increased or injection timing is delayed.

Thus, the main objective of this work was to compare different engine strategies to enhance the late cycle mixing controlled combustion process and therefore to improve the soot oxidation process while maintaining similar gross indicated efficiency in a light-duty engine. For this purpose, a simplified methodology defined in [14] was used, which analyzed the effect of mixing process and in-cylinder bulk gas temperature on soot oxidation during the late cycle combustion. Experimental measurements were made in a single-cylinder direct-injection light-duty diesel engine varying the swirl ratio and the injection pattern as injection pressure, Start of Energizing (SoE), Energizing Time (ET) and number of injections events. To analyze soot, the optical thickness (KL) parameter was used, which was measured by an optoelectronic probe based on the two-color pyrometry method. The apparent combustion time (ACT^{-1}) was used as mixing tracer. This parameter is based on the injection rate profile and the experimental heat release. Finally, both strategies (swirl ratio and injection pattern) were evaluated with the goal of getting the maximum benefits in terms of the soot oxidation process.

2. EXPERIMENTAL TOOLS

2.1.Test cell and engine description

The experimental measurements were carried out in a single-cylinder light-duty diesel engine. It was equipped with a common-rail fuel injection system and a high-pressure exhaust gas recirculation. This engine is derived from a production GM 1.9L Diesel engine, which has four valves per cylinder, centrally located injector and a re-entrant type piston bowl. For performing this research, the engine was modified with two swirl flaps in the air intake port, which allowed for a variation in swirl ratio from 0 to 5. The important engine data as well as the injection system information are given in the table 1.

Engine Type	DI, 1-cylinder, 4-stroke	**Max. Power [kW]**	27.5 @ 4000 rpm
		Max. Torque [Nm/min^{-1}]	80 @ 2000-2750 rpm
Displacement[mm^3]	477	**Injection System**	Bosch Common Rail (solenoid)
Stroke [mm]	90.4	**Max. Rail Pressure [bar]**	1600
Bore [mm]	82	**Nozzle hole diameter [mm]**	0.141
Combustion Chamber	Re-entrant type	**Injector Nozzle Holes**	7
Compression ratio	17.1:1	**Hydraulic flow rate [cm^3 (30s) at 100 bar]**	440

Table 1. Engine and injection system specifications

The single cylinder engine was installed in a fully instrumented test cell with an auxiliary facility necessary for the operating, control and acquisition of raw data. Figure 2 shows the complete test-cell scheme.

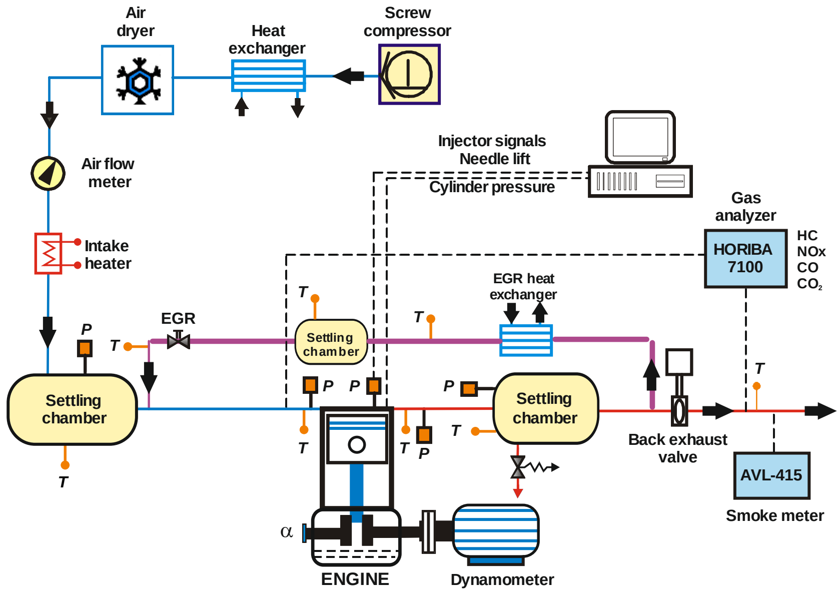

Figure 2. Complete test cell set-up

The engine was connected to an electric dynamometer, to control engine speed and load. To reach the desired intake air flow conditions, an externally driven screw compressor was used to provide the necessary boost pressure before passing through the air dryer system to control the relative humidity air. The air pressure and temperature were regulated inside of intake settling chamber after mixing the EGR. The exhaust backpressure was adjusted by means of a pneumatic valve to simulate the effect of the turbocharger in the real engine. The exhaust pressure and temperature were controlled in the exhaust settling chamber.

The concentrations various constituents in the exhaust gas were analyzed with a five gas Horiba MEXA-7100 DEGR analyzer bench. To assure the accuracy of the measurements, the different pollutant species were measured and averaged over 60 seconds after attaining steady state operation. The smoke emissions were measured with an AVL 415 variable sampling smoke meter. Three consecutive measurements (1 litre volume each sample) were acquired and averaged supplying results directly in FSN (Filter Smoke Number) units [21].

The in-cylinder pressure was measured during 400 consecutive cycles with a Kistler 6125C glow-plug piezoelectric transductor coupled to a 4603B10 charge amplifier. The pressure signal was measured every 0.5º by a Yokogawa DL708E oscillographic recorder with a 16 bits A/D converter module. The common-rail fuel injection system was managed by a commercial DRIVVEN controller system [22]. The mean variables were acquired at a low sampling frequency of 100 Hz using SAMARUC, a CMT-developed test system that collects the signals of different sensors and controls the electric dynamometer [23].

2.2. Optoelectronic probe

The in-cylinder soot data were measured with an AVL optoelectronic signal converter based on the two color method, known as AVL VisioFEM with a selection of photodiodes and narrow band optical filters adapted for IC engines. Figure 3 shows a scheme of the light probe. At the tip of the probe, a sapphire lens records the luminous intensity from the flame in the combustion chamber with an angle view of 90º. The light is transported through optical fiber and it is split to two filters at wavelength of 600 and 950 nm (around ±50nm FWHM each one). Photodiodes convert the intensity to a voltage signal. This is amplified and acquired every 0.5º CAD. The raw signals of the optoelectronic probe are referenced with a halogen lamp mounted to an integrating sphere, which provides a homogenously illuminated surrounding. The transmission of the light probe is obtained with the halogen lamp base by a methodology provided by AVL. Each operating point was recorded with 4 repetitions of 100 combustion cycles (400 cycles).

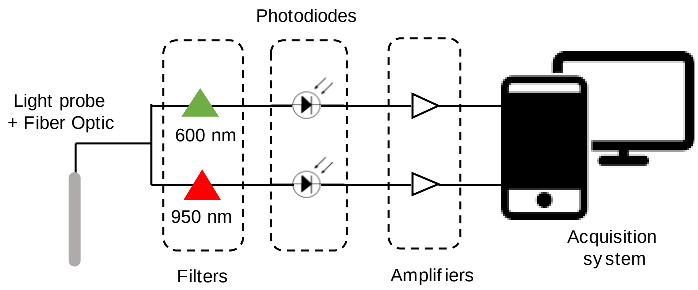

Figure 3. Signal path from flame to data acquisition device

Once the temporal evolution of the raw voltage signal was determined, the spectral emission was calculated with the equation (1):

$$I_{soot}\left[\frac{W}{m^2\cdot m\cdot sr}\right] = \frac{Voltage\ signal\ [V]\cdot Sensitivity\ [\frac{W}{m^2\cdot m\cdot sr\cdot V}]}{Gain\ [-]\cdot Transmission[-]} \qquad (1)$$

where I_{soot} is spectral emission, temporal voltage signal for each wavelength (600 and 950 nm) recorded by the optoelectronic probe, sensitivity is a constant of the pyrometer and thus, the manufacturer provides it. The gain was fitted during the measured process according to the light intensity.

Finally, the two color method was applied for obtaining the temperature and soot volume fraction (KL). This technique establishes that the spectral emission emitted by the soot particles (I_{soot}) inside the combustion chamber is proportional to the intensity emitted by a black body at the same temperature (equation 2). The proportional factor is determined by the emissivity of the soot particles, which depends on the soot concentration, working wavelength (λ).

$$I_{soot}\,(\lambda, T, KL) = \varepsilon_\lambda I_{b,\lambda} = \left[1 - exp\left(-\frac{KL}{\lambda^\alpha}\right)\right]\frac{1}{\lambda^5}\frac{c_1}{\left[exp\left(\frac{c_2}{\lambda T}\right)-1\right]} \qquad (2)$$

Where c_1 = 1.1910439 x 10-16 Wm^2sr^{-1} and c_2 = 1.4388 x 10^{-2}mK. Zhao et al. [22] reported that α values are less dependent on the wavelength in the visible range than in the infrared.

For the sake of clarity, figure 4 presents the optical set up when the optoelectronic pyrometer is used in the light duty engine. In this figure, the piston is located at 20 CAD after top dead center. It is possible to observe the injector, the optoelectronic flush mounted probe as well as its field of vision in the combustion chamber.

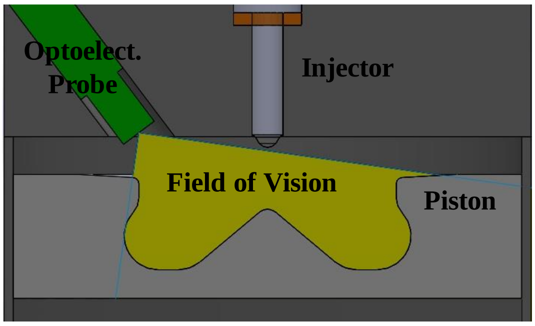

Figure 4. Optoelectronic pyrometer set up on the light duty engine configuration

2.3. Test Matrix

In this research, a study was carried out for evaluating the potential of swirl ratio and a dedicated injection strategy to enhance the late cycle mixing controlled combustion. For that, a reference operating condition was selected as baseline case for analyzing the effect of each strategy on the late cycle combustion and finally, to compare both strategies for selecting the best option. The engine was operated maintaining constant engine speed at 2000 rpm and low load at 5 bar BMEP considering the flame transparency uncertainties imposed by the two-color method [14].

In addition, the temperature of the coolant and oil stayed constant for all the measurements at 86ºC and 95ºC, respectively. For each operating condition, 4 repetitions were measured and the results were averaged in order to minimize the experimental uncertainties.

2.3.1. Baseline case

The experimental engine operating conditions are represented in table 2. These operating conditions were chosen for being representative of typical operating point for the derived production GM 1.9L Diesel engine, which was set up to meet EURO IV emissions regulations.

Operation condition	**Baseline case**		
Injection pressure [bar]	650	**T_{in} [K]**	318
Fuel Flow [kg/min]	0.018	**P_{in} [bar]**	1.306
SoE [ºBTDC]	19.5 / 9.9 / 0.3	**P_{exh} [bar]**	1.49
ET [ms]	0.310 / 0.310 / 0.587	**Air Flow [kg/min]**	0.659
		EGR [%]	0
SR [-]	1.5	**CA50 [º aTDC]**	13

Table 2. Baseline engine operating conditions

2.3.2. Engine setting sweeps

Table 3 presents the text matrix for the two different strategies studied in this work. In the first strategy, the objective was to evaluate the effect of swirl ratio on late-cycle combustion process. For that, the swirl ratio was varied from 0 up to 5, in steps of 1 unit maintaining constant all other engine parameters The tests were performed with the same trapped mass at the IVC. For that, the intake pressure was adapted in every test. While, the intake air temperature and the exhaust pressure were kept constant. Regarding the injection pattern, all parameters were kept constant except the SoE and ET for the main injection event, which were modified for obtaining the same CA50 and fuel mass in all cases.

Operation condition	SR Sweep	Injection Strategy Optimization
Injection pressure [bar]	650	800
Fuel Flow [kg/min]	0.018	
SoE [ºBTDC]	19.5 / 9.9 / 0 - 0.5	19.2 / 9.6 / -0.5 / -4.7
ET [ms]	0.310 / 0.310 / 0.582 - 0.590	0.285 / 0.300 / 0.510 / 0.150
Number of Injections	3 (2 pilots and 1 main)	4 (2 pilots, 1 main and 1 post)
SR [-]	0 - 5	1.5
T_{in} [K]	318	
P_{in} [bar]	1.300 - 1.410	1.304
P_{exh} [bar]	1.475	
Air Flow [kg/min]	0.659	
EGR [%]	0	
CA50 [º aTDC]	13	

Table 3. Experimental engine operating conditions

The aim of the second strategy was to produce the same RoHR for the high swirl case (SR=3), which implies the highest GIE. The baseline case was taken as reference point. To achieve the same RoHR, the parameters CA10, CA25, CA50, CA75 and CA90 must be very similar. Thus, some considerable changes of the injection strategy (injection pressure, duration and position of each injection and number of injection) were applied as table 3 shows.

Commercially available European diesel fuel was used for this work. Table 4 shows the main characteristics of the fuel used.

Fuel	Diesel
Cetane Number	50.8
Density @ 313K [kg/m^3]	820
Distillation @ 65/ 85/ 95% [K]	568.3 / 601.4 / 624
HC Ratio	6.05
Weight Molecular [g/mol]	215.42
Dynamic Viscosity @ 313K [cSk]	2.38

Table 4. Fuel properties at 1 atm and 40ºC

3. THEORETICAL TOOLS

3.1. 0-D model: Calmec

A 0-D single-zone thermodynamic model, called CALMEC, was used to perform the combustion analysis. This model is completely described in [25]. The in-cylinder pressure signal was the main input for the combustion analysis. The signal was measured with a pressure transducer linked with its corresponding charge amplifier. The pressure signal was measured from 400 consecutive combustion cycles to avoid the experimental uncertainties due to the cycle-to-cycle variation. Each individual raw pressure data was smoothed by means of a low-pass filter. Once all recorded cycles were filtered, the set of cycles was averaged in order to create a representative in-cylinder pressure trace, which was used to carry out the combustion analysis. The first law of thermodynamics was applied between IVC and EVO (during the closed cycle), considering the combustion chamber as an open system because of the blow-by and fuel system. In addition, the ideal gas equation of state was used to calculate the average gas temperature in the combustion chamber [26]. The main output of this tool was the RoHR, which allowed for calculating other important parameters such as Start of Combustion (SoC).

3.2. Apparent Combustion Time Concept

The Apparent Combustion Time (ACT) parameter was used to evaluate the amount of mixing during the combustion process [27]. Figure 5 illustrates that this parameter can be defined as the time interval between the instant when a determined percentage of the mass injected (point of injection, POI_i) and the instant when the same percentage of fuel mass is burned (point of combustion, POC_i). In a diffusion combustion process, it is noted that if a certain fuel mass is considered as a physical package, this package will not burn instantaneously at the instant POC. It will probably start to burn before the instant POC and it will finish burning after the instant POC. Therefore, the ACT (defined as ACT=POC-POI) has been considered as an approximation of the average time interval elapsed between the injection and the combustion for a particular fuel mass package. The ACT concept must be distinguished from the ignition delay. ACT matches with the ignition delay only in the first fuel injected package as figure 5 shows. Besides, the mixing time is different for the first fuel package and the last fuel package. Due to deterioration of the local thermodynamic conditions (gas density and oxygen molar fraction mainly), ACT presents an enlargement in its value when combustion process is evolving. Figure 6 presents the temporal evolution of ACT (dashed blue line), which corresponds to the case showed in the figure 5. In addition, ACT^{-1} parameter is also presented in the figure 6. This parameter can be considered as a mixing capability tracer.

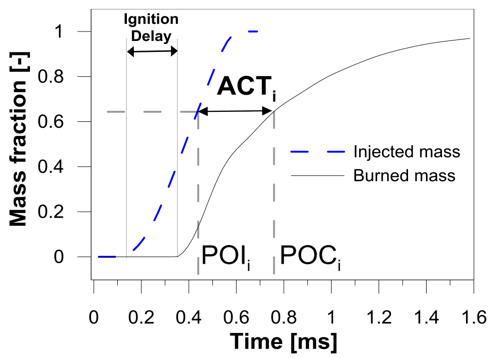

Figure 5. Definition for the Apparent Combustion Time (ACT)

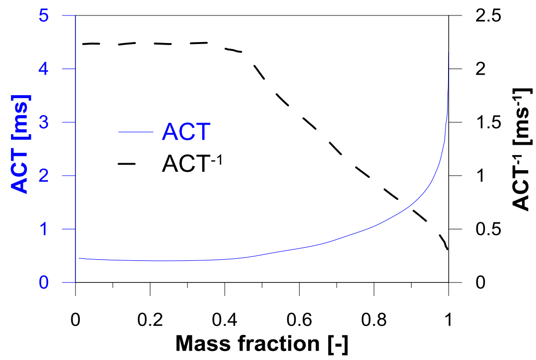

Figure 6. Evolution of the ACT and ACT^{-1} parameter for the case shown in previous figure (single injection pulse)

4. RESULTS AND DISCUSSIONS

4.1. Impact of swirl ratio on late cycle combustion

An increase in swirl ratio causes an improvement in turbulence and vorticity due to the higher rotational speed of the air flow and therefore, an acceleration of combustion rate [28].

Figure 7 shows the apparent combustion time (ACT^{-1}) parameter at 90% of total heat released for the swirl ratio sweep, ranged from 0 to 5. This parameter was used as a mixing capability tracer during the late cycle (from EoI up to EoC). Thus, it can be said that the values present an increase in mixing capability when the swirl ratio raises up to a maximum and later, a decrease in mixing parameter is produced. From SR= 3, the increase in swirl ratio produces presumably a deterioration of the combustion development due to excessive spray interaction and/or a displacement of the combustion process towards the squish region [29]. In this sense, it is possible to state that SR= 3 is the best condition in terms of mixing capability.

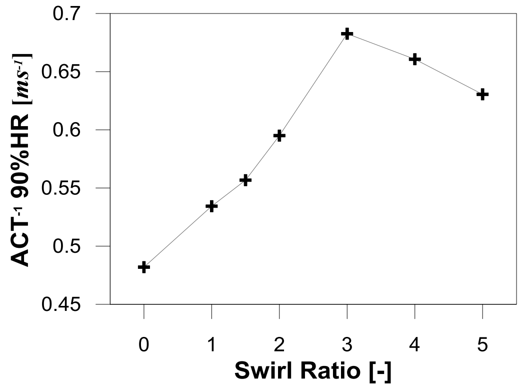

Figure 7. ACT^{-1} parameter at 90% of heat release for each swirl ratio at 2000rpm at 5bar BMEP.

Figure 8 (left) represents the maximum values of RoHR for the same swirl ratio sweep. When the swirl ratio increases, the peak of RoHR is higher due to a faster mixing process up to the SR=3 (maximum mixing capability) due to an enhancement in the combustion process. The figure (right) indicates the interval duration (in CAD) from 70 to 80% and 80 to 90% of the total heat release, respectively. These intervals represent approximately the late cycle part of combustion event. The chart shows a reduction in both interval durations when the swirl ratio is increased. It indicates that there is higher energy released during expansion stroke, resulting a better thermal efficiency.

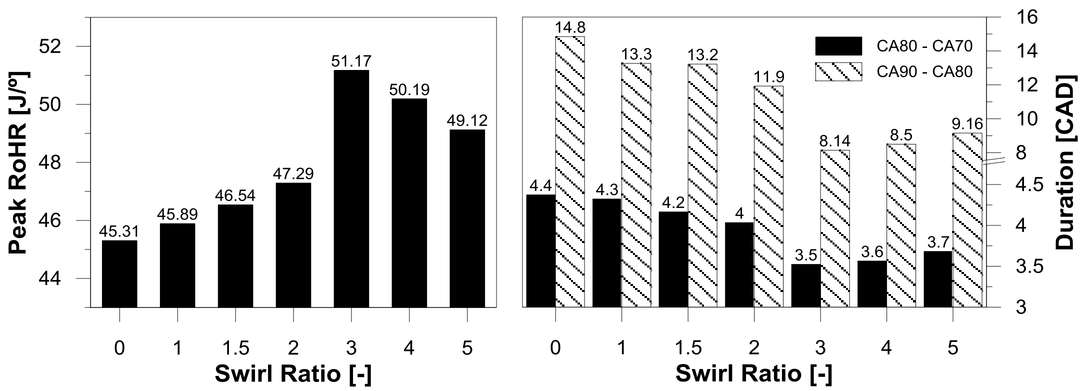

Figure 8. Peak of RoHR and interval duration for swirl ratio sweep at 2000rpm at 5bar BMEP.

According to the conclusion obtained in the previous figures, it is possible to conclude that, when SR is increases, the Gross Indicated Efficiency (GIE) should also be increased as shown the figure 9. This figure presents the Gross Indicated Efficiency for seven different swirl ratios. The trend is similar as figures 7 and 8. Finally, the SR= 3 condition is selected as optimum point considering that is the best SR condition for swirl sweep in terms of mixing capability, combustion process and GIE.

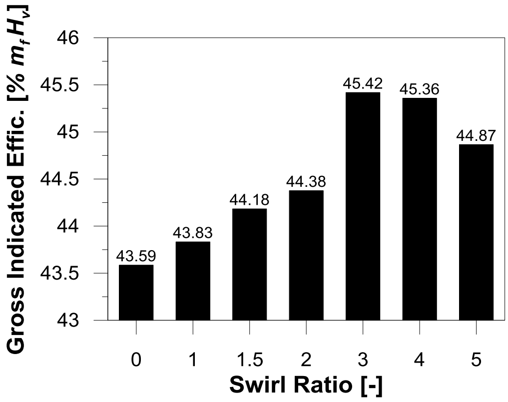

Figure 9. Gross Indicated Efficiency for different swirl ratios.

Once the “optimum” SR has been selected, the main goal of this section is to study the impact of SR on the soot oxidation process during the late cycle combustion, since the oxidation plays the main role in the final engine-out soot emissions. For this purpose, it was analyzed how the mixing process and bulk gas temperature affect to oxidation process for optimum SR compared with the baseline condition. For that, two tracers were used: on the one hand, the half-life time of ACT^{-1} evaluated the mixing capability and its effects on combustion process (and exhaust emissions), and on the other hand, the half-life time of optical thickness (KL) was proposed with the goal of evaluating the reduction in soot after de EoI. In addition, the average bulk gas temperature during the late cycle was also added to better understand the soot oxidation phenomenon.

Figure 10 (left) shows the temporal evolution of ACT^{-1} and its exponential fit (discontinuous line) for the baseline (SR=1.5) and optimum (SR= 3) conditions. Each curve represents the average of 400 cycles. The ACT^{-1} curves have been drawn after EoI due to the late cycle combustion covered from EoI up to End of Combustion (EoC).

By definition, the half-life time of exponential ACT^{-1} curve is given by:

$$ACT^{-1} = b \cdot e^{\frac{-\ln(2) \cdot x_{CAD}}{t_{1/2}}} \qquad (3)$$

where b is a constant and x_{CAD} is the crank angle position aTDC in CAD. Then, the half-life time concept was defined as the necessary time for the initial value for the variable (in this case, ACT^{-1}) decrease up to its half value.

Table 5 indicates the interval in which the ACT^{-1} curves has been fitted and the R^2-values for the experimental fits. The exponential fits start around 13 CAD aTDC (approximately the EoI) up to the point when the profiles approach zero.

ACT^{-1}		
Point	Interval fitting [CAD]	R^2-values
Baseline (SR= 1.5)	12.6 - 31	0.9747
SR= 3	12.6 - 33	0.9852

Table 5. Interval fitting analyzed and R^2-values for the experimental fits to ACT^{-1} trace at different swirl level cases.

The figure 10 (right) represents the results of half-life times of ACT^{-1} for the baseline and optimum SR case. When the swirl ratio increases, the half-life time of ACT^{-1}, $t_{1/2\ ACT^{-1}}$, is reduced and so, the mixing process is improved. Maintaining constant conditions at intake closing (air intake temperature and mass, without EGR) and the injection strategies for both measured points, a higher value of swirl ratio is expected to enhance turbulence and vorticity [17]. These phenomena explain a lower time to burn similar amount of injected fuel. So, an improvement in the air/fuel mixing process was confirmed.

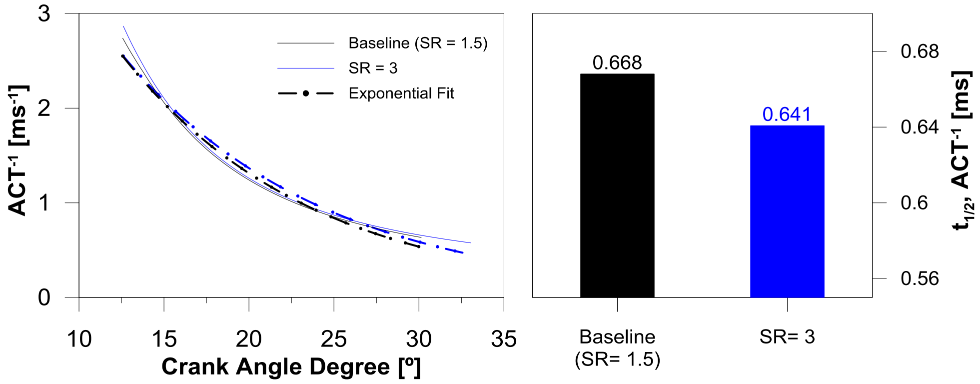

Figure 10. Temporal evolution of ACT^{-1} and its exponential fits (left) and half-life times of ACT^{-1} (right) obtained for different swirl level cases.

Figure 11 shows the time evolution of gas temperature (left) and average bulk gas temperature (right) for the baseline and SR= 3 cases. This average was calculated in the same range as previously used to fit the half-life time of ACT^{-1}. Each curve represents the average of 400 cycles. As other researchers report [14], the bulk temperature has an important effect by increasing the reaction rates. Averaged bulk gas temperature value is higher for the SR=3 (approximately 100K). At higher temperatures, the soot oxidation process is expected to be enhanced in the flame sheath and then, it leads to a reduction in a both in-cylinder soot and exhaust particulate emissions.

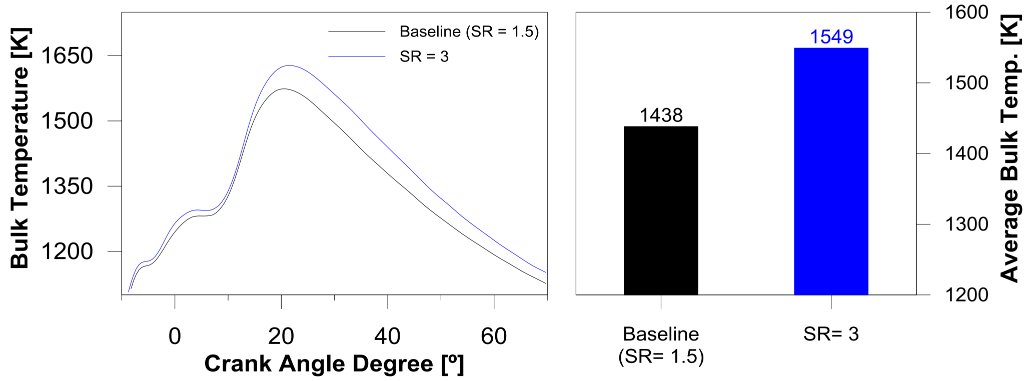

Figure 11. Temporal evolution of bulk gas temperature (left) and averaged bulk gas temperature (right) obtained for different swirl level cases.

For evaluating the soot oxidation process, the half-life time parameter has been used considering that KL curves take an exponential shape after the EoI. The half-life time of KL was adjusted by an exponential fit and it is given by the following equation:

$$KL = c \cdot e^{\frac{-\ln(2)\cdot x_{CAD}}{t_{1/2}}} \qquad (4)$$

where c is constant and x_{CAD} is the crank angle position aTDC in CAD. So, the half-life time of KL was determined as the time in which the soot concentration is reduced up the half its initial value. Table 6 indicates the interval in which the KL curves have been fitted and the R^2-values for the experimental fits. Due to higher swirl, the peak of KL is closer the TDC than to the baseline and therefore, the onset of exponential fit is located at different crank angle intervals.

KL		
Point	Interval fitting [CAD]	R^2-values
Baseline (SR=1.5)	21 - 54	0.9503
SR= 3	11 - 51	0.9786

Table 6. Interval fitting analyzed and R^2-values for the experimental fits to KL trace for the different swirl level cases.

Figure 12 (left) represents temporal evolution of KL and its exponential fit and the results of half-life times of KL for the baseline and SR=3 case (right). Each curve represents the average of 400 cycles. As it was expected [17], the half-life time of KL decreases with the increase of swirl number, maintaining constant the rest of variables. For the optimum SR case, the in-cylinder angular velocity is higher than the baseline. The enhanced turbulence and vorticity produces a higher soot oxidation rate for the SR= 3 case independently on the initial soot concentration.

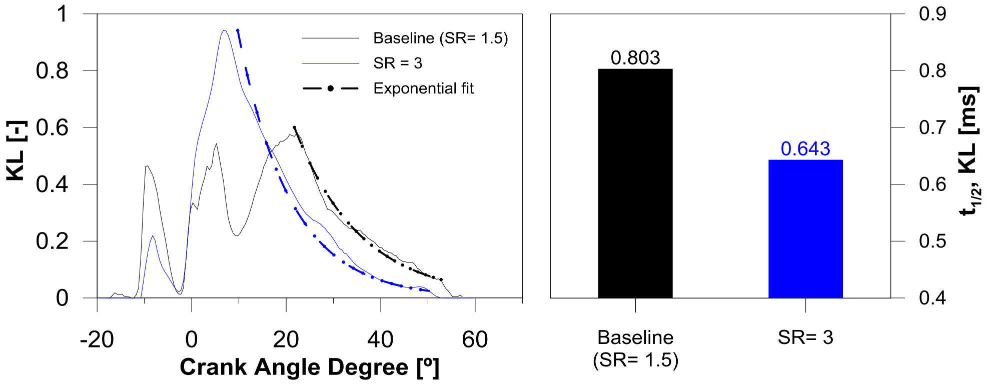

Figure 12. Temporal evolution of KL and its exponential fits (left) and half-life times of KL (right) obtained for different swirl level cases.

4.2. Impact of injection pattern on late cycle combustion

The post-injection is a shorter injection pulse that follows the main injection, which improves the mixing process and increases the temperature during the late cycle combustion phase. Thus, the post-injection enhances soot oxidation leading to a reduction in the engine-out soot emissions [30]. The effects of injection pressure and post injections are well-known on the combustion process. An increase in injection pressure causes an equivalence ratio reduction at the lift-off length (LOL) and thus, a reduction in soot formation [10]. In the current section, the aim is to obtain similar RoHR to SR=3 (optimum GIE case) by using a reduced swirl ratio (baseline SR= 1.5 case) condition by modifying only the injection settings (number of injection, injection pressure and duration and position of each injection event).

Figure 13 explains how the injection settings were determined to obtained the similar RoHR. Thus, to replicate the RoHR obtained with the highest swirl ratio tested using the lowest swirl, different steps were proposed. First, the injection pressure was increased in steps of 50 bar. Faster RoHR with higher peak was obtained after this process. In the following step, the Start of Energizing (SoE) times, as well as the Energizing Times (ET), were changed to adjust the CA10, CA25 and CA50 parameter for both operating conditions (SR= 3 and post-injection case at SR = 1.5). Finally, a post injection event was added to compensate the better mixing process at the late cycle combustion phase achieved with the optimum SR=3 case. With this proposal, the differences between CA75 and CA90 were acceptable (less 2º CAD).

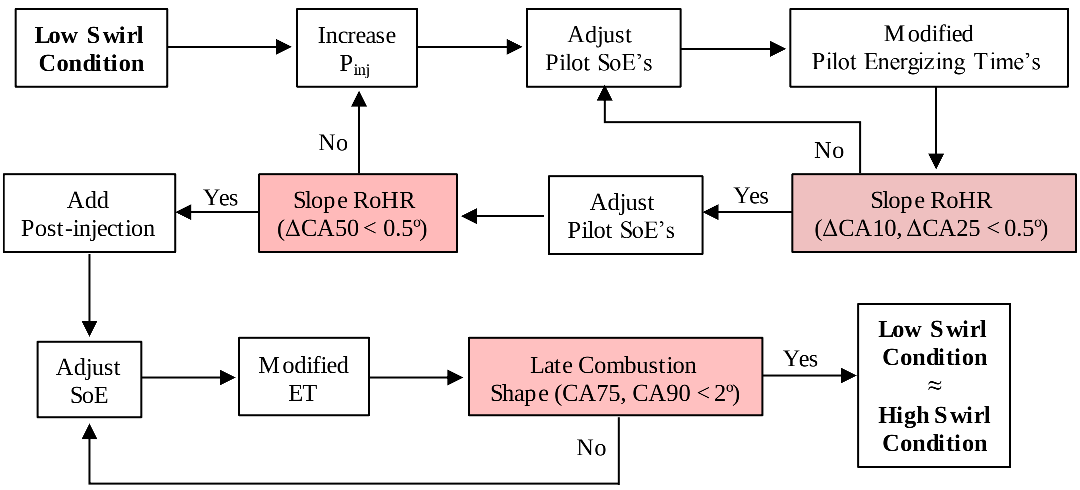

Figure 13. Experimental methodology used to get similar RoHR of SR= 3 with baseline condition (SR=1.5).

Figures 14, 15 and 16 evaluate the mixing and combustion processes of the post injection case at the baseline SR of 1.5 compared to the optimum (SR= 3) case.

Figure 14 shows the apparent combustion time (ACT^{-1}) parameter at 90% of total heat release for baseline, optimum and post injection cases. It is possible to note that the post injection case presents a similar mixing capability to the SR=3 case and, as it has been explained in the previous sub-section, both operating conditions show an increase in mixing capability when compared to the baseline case.

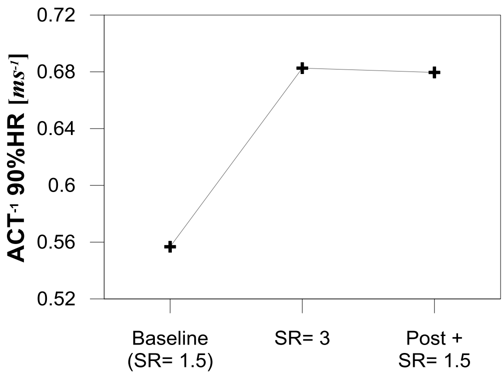

Figure 14. ACT^{-1} parameter at 90% of heat release for the baseline, optimum SR and post injection case.

In addition, the peak of RoHR is slightly higher at SR= 3 than the post injection case (approximately 1 J/º) as shown in the figure 15. This fact could be due to the small differences in the RoHR fit. Considering the interval duration from 70 to 80% and 80 to 90 % of the total heat release, the trend follows the same shape. The values of SR= 3 and post-injection case are very similar and the interval durations are shorter compared to the baseline case.

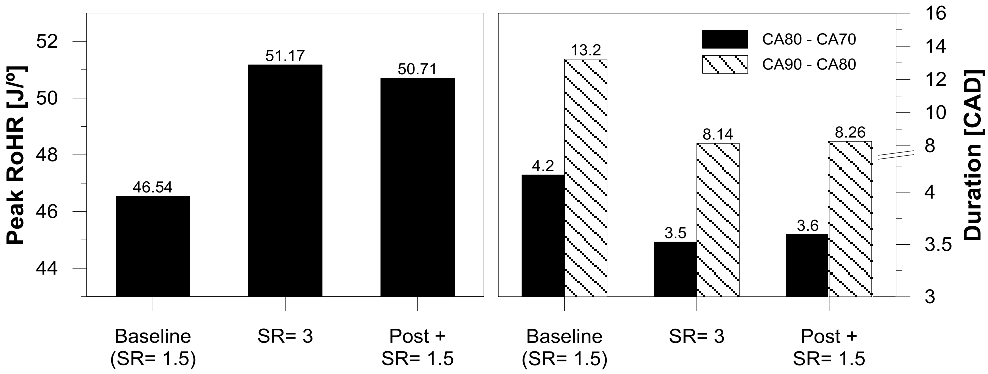

Figure 15. Peak of RoHR and interval duration for the baseline, optimum SR and post injection case.

Figure 16 presents the GIE for the three different operating conditions. According to the conclusion obtained in the two previous figures, SR= 3 and post injection case present similar values of GIE. It can be therefore concluded that the selected injection strategies replicate the optimum case (SR= 3).

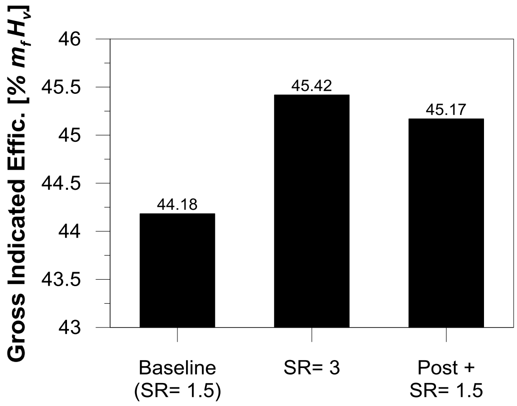

Figure 16. Gross Indicated Efficiency for the baseline, optimum SR and post injection case.

Once the post injection case has been selected, it is necessary to study the impact of the injection pattern on the soot oxidation during the late cycle combustion. Following similar work scheme as the swirl ratio section, the relationship of mixing process and bulk gas temperature on the soot oxidation process for post injection and baseline cases was studied.

Figure 17 (left) shows the temporal evolution of ACT^{-1} and its exponential fit (discontinuous line) for the baseline and post injection conditions. Each curve represents the average of 400 cycles. The crank angle ranges and R^2-values for the exponential fit are presented in table 7. Figure 17 (right) presents the half-life times of ACT^{-1} for the baseline and post injection case. The half-life of ACT^{-1} with the post injection pulse is lower than the baseline case due to mainly two phenomena: the injection pressure and the post injection event. On the one side, if the injection pressure increases, the half-life time of ACT^{-1} is reduced. A higher injection pressure produces an increase in the movement of the in-cylinder air environment due to the higher momentum of the spray and so, this air movement enhances the air/fuel mixing process during the late cycle combustion [14]. On the other side, the mixing process is improved by adding the post injection. The post injection redistributes the fuel from the main injection, generating a more well mixed air/fuel distribution [19].

ACT^{-1}		
Point	Interval fitting [CAD]	R^2-values
Baseline (SR=1.5)	12.6 - 33	0.9747
Post + SR=1.5	12.1 - 33	0.9299

Table 7. Interval fitting analyzed and R^2-values for the experimental fits to ACT^{-1} trace for the different injection pattern

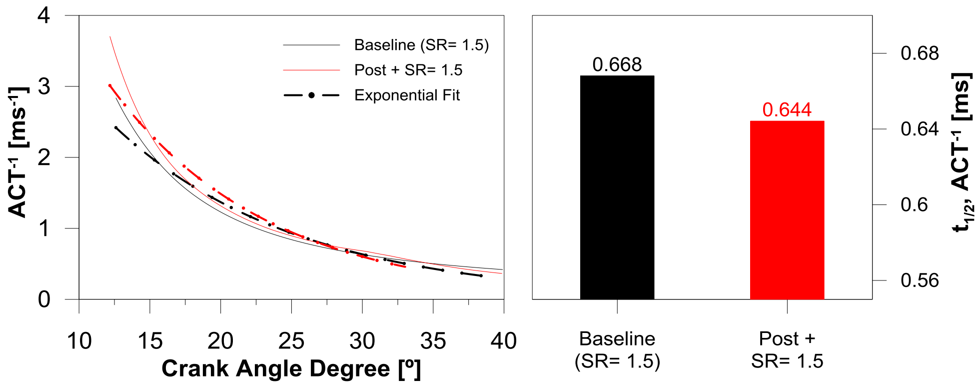

Figure 17. Temporal evolution of ACT^{-1} and its exponential fits (left) and half-life times of ACT^{-1} (right) obtained for different injection pattern

Figure 18 shows temporal evolution of gas temperature (left) and average bulk gas temperature (right) during the late cycle for the baseline and post injection conditions. Each curve represents the average of 400 cycles. The average bulk temperature for the post injection case is higher than the baseline case (around 100K). As in the previous sub-section, soot oxidation process is enhanced when the bulk gas temperature is higher.

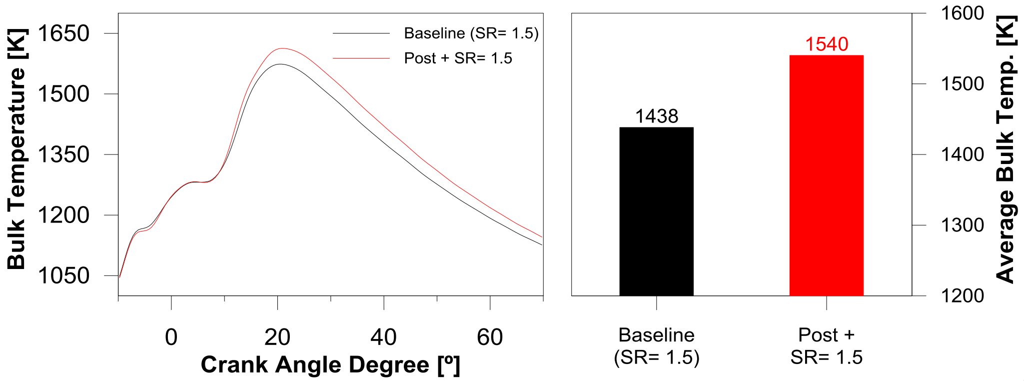

Figure 18. Temporal evolution of bulk gas temperature (left) and averaged bulk gas temperature (right) obtained for different injection pattern.

Once the mixing process and bulk gas temperature were studied, it was necessary to evaluate the soot oxidation process.

Figure 19 (left) represents temporal evolution of KL and its exponential fit for the baseline and post injection cases. Each curve represents the average of 400 cycles. The selected crank angle ranges for the exponential fit and R^2-values are presented in table 8. Figure 19 (right) shows the results of half-life times of KL for the baseline and post injection case. As expected, the half-life time of KL for the post injection case was lower than the baseline case. An increase in injection pressure enhances the mixing process during the late cycle combustion and thereby, the soot oxidation process. As other researches have reported in the literature [31, 32], post injection enhances mixing of soot from the main injection and available in-cylinder air/O_2 and the oxidation of this soot is enhanced due to combustion of the post-injection fuel.

KL		
Point	Interval fitting [CAD]	R^2-values
Baseline (SR= 1.5)	21 - 54	0.9503
Post + SR= 1.5	12 - 51	0.9742

Table 8. Interval fitting analyzed and R^2-values for the experimental fits to KL trace for the different injection pattern.

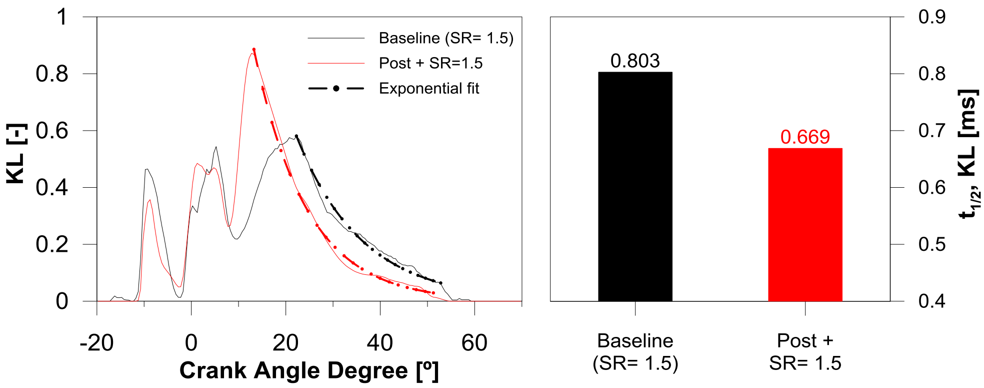

Figure 19. Temporal evolution of KL and its exponential fits (left) and half-life times of KL (right) obtained for different injection pattern.

4.3. Emissions comparison of optimized swirl ratio and post injection strategies on late cycle combustion

Once the soot oxidation has been analyzed independently for the two different strategies versus the baseline case, this section aims to compare the optimum swirl ratio and post injection cases during the late cycle combustion. This comparison has been used to identify the best engine strategy.

Figure 20 (left) shows the engine-out NOx and soot emissions for baseline, optimum SR and post-injection conditions. The expected soot-NOx trade-off is found. Considering that combustion process between optimum SR and post injection case is quite similar, it is also expected to have similar engine-out emissions. A negligible difference in NOx emission (approximately 0.7 g/kg fuel) was measured. In addition, these conditions present higher values than the baseline case. This fact is maybe due to a faster combustion process and thus higher local combustion temperatures for the maximum GIE cases than the baseline case. Regarding soot emissions, it is interesting to remark that the post-injection soot is quite similar to the SR= 3 case and significantly lower than the baseline case due to an improvement of mixing and oxidation processes.

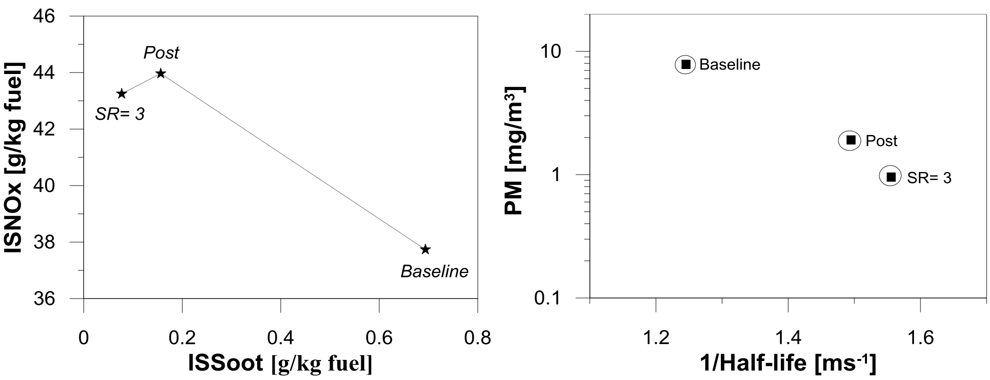

Figure 20. Left) The ISNOx vs ISSoot emissions for the 3 different point at 2000rpm@ 5bar BMEP. Right Soot emissions versus half-life time of KL for each swirl ratio at 2000rpm at 5bar BMEP

Figure 20 (right) presents engine-out emissions versus the inverse of half-life time of KL ($1/t_{1/2,KL}$) on a semi-logarithmic scale for swirl ratio sweep and post-injection case. The three conditions studied in this research have been marked with black circles. It is observed that the soot emissions are drastically reduced for the SR= 3 and post injection cases, where the soot oxidation rate (and mixing capability) was improved. A linear relationship is stablished between the soot emissions and the oxidation rate. Therefore, engine-out soot emissions are governed mainly by oxidation process. In conclusion, it is possible to improve the late cycle diffusion combustion (and thus, soot oxidation process) with an appropriate injection strategy for a low SR condition.

5. CONCLUSIONS

The main objective of this work was to compare different engine strategies to enhance the late cycle mixing controlled combustion process and therefore, to improve the soot oxidation while maintaining similar gross indicated efficiency. The experimental measurements were made in a light-duty engine by modifying the swirl ratio and the injection strategy. In particular, experimental and theoretical parameters were used to carry out the research. The apparent combustion time (ACT^{-1}) was used as mixing tracer. An exponential fit was applied to the temporal evolution of ACT^{-1}. This parameter is based on the injection rate profile and the experimental heat release. The soot oxidation process was evaluated with an exponential fit applied to the temporal evolution of optical thickness (KL). KL was obtained by applying the two color method using a dedicated optoelectronic pyrometer. Finally, both strategies (swirl ratio and injection pattern) were compared in terms of engine-out emissions. The conclusions of the study can be summarized as follows:

- An increase in swirl ratio is not directly related with an increase in mixing process during the late cycle combustion. Indeed, an excessive SR can lead a deterioration of the combustion development due to excessive spray interaction, which causes a slower and less powerful heat release process reducing the indicated efficiency.
- Half-life time of KL was revealed as a proper tracer for characterizing soot emissions in CI engines. This parameter is governed by mixing capability (half-life time of ACT-1) and bulk gas temperature. When half-life of ACT-1 is reduced due to higher SR and/or injection pressure and/or post injection addition, the average bulk gas temperature is increased. Both phenomena cause an improvement in the soot oxidation process (reducing half-life of KL).
- A proper injection pattern (increase of injection pressure and post injection addition) coupled with a low SR was showed as a suitable strategy to improve the late cycle diffusion combustion as well as soot oxidation while maintaining constant GIE.
- According to the emission results obtained, the expected soot-NOx trade-off was found. So, considering that combustion process between optimum SR = 3 and post injection case was quite similar, it was also expected to have similar engine out emissions. Thus, the soot reduction can be attained with higher swirl ratio and a proper injection strategy. On the contrary, NOx emissions increased appreciably when the mixing process is enhanced (SR = 3 and SR=1.5 adjusted). In addition, a linear relationship was stablished between the soot emissions and the soot oxidation process, which indicates that mainly the soot oxidation process governs the engine-soot emissions.

REFERENCES

[1] Desantes J., Benajes J., Molina S., Gonzalez C.A. The modification of the fuel injection rate in heavy-duty diesel engines. Part 1: Effects on engine performance and emissions. Applied Thermal Engineering Volume 24, Issues 17–18, December 2004, Pages 2701–2714. doi.org/10.1016/j.applthermaleng.2004.05.003.

[2] Desantes J., Benajes J., Molina S., Gonzalez C.A. The modification of the fuel injection rate in heavy-duty diesel engines: Part 2: Effects on combustion. Applied Thermal Engineering Volume 24, Issues 17–18, December 2004, Pages 2715–2726. doi.org/10.1016/j.applthermaleng.2004.05.004.

[3] Desantes J., Arrègle J., López J., García A. A Comprehensive Study of Diesel Combustion and Emissions with Post-Injections. SAE Technical Paper 2007-01-0915, 2007, doi: 10.4271/2007-01-0915.

[4] Benajes J., García A., Monsalve-Serrano J., Boronat V., Achieving clean and efficient engine operation up to full load by combining optimized RCCI and dual-fuel diesel-gasoline combustion strategies. Energy Conversion and Management, Volume 136, 15 March 2017, Pages 142-151. doi.org/10.1016/j.enconman.2017.01.010.

[5] Gallo, Y., Simonsson, J., Lind, T., Bengtsson, P. et al. A Study of In-Cylinder Soot Oxidation by Laser Extinction Measurements During an EGR-Sweep in an Optical Diesel Engine. SAE Technical Paper 2015-01-0800, 2015, doi:10.4271/2015-01-0800.

[6] Benajes J., Olmeda P., Martín J., Blanco-Cavero D., Warey A. Evaluation of Swirl Effect on the Global Energy Balance of a HSDI Diesel Engine. Energy, Volume 122, 1 March 2017, Pages 168-181. dx.doi.org/10.1016/j.energy.2017.01.082.

[7] Garcia A., Monsalve-Serrano J., Heuser B., Jakob M., Kremer F., Pischinger S. Influence of fuel properties on fundamental spray characteristics and soot emissions using different tailor-made fuels from biomass. Energy Conversion and Management, Volume 108, 15 January 2016, Pages 243-254. doi.org/10.1016/j.enconman.2015.11.010.

[8] Benajes J., García A., Pastor J. M., Monsalve-Serrano J. Effects of piston bowl geometry on Reactivity Controlled Compression Ignition heat transfer and combustion losses at different engine loads. Energy, Volume 98, 1 March 2016, Pages 64-77. doi.org/10.1016/j.energy.2016.01.014.

[9] Benajes J., García A., Monsalve-Serrano J., Balloul I., Pradel G. An assessment of the dual-mode reactivity controlled compression ignition/conventional diesel combustion capabilities in a EURO VI medium-duty diesel engine fueled with an intermediate ethanol-gasoline blend and biodiesel. Energy Conversion and Management, Volume 123, 1 September 2016, Pages 381-391. doi.org/10.1016/j.enconman.2016.06.059.

[10] Benajes J., Martín J., García A., Villalta D., Warey A. In-cylinder soot radiation heat transfer in direct-injection diesel engines. Energy Conversion and Management, Volume 106, December 2015, Pages 414–427, doi:10.1016/j.enconman.2015.09.059.

[11] Pickett L.M., Siebers D.L. Soot in diesel fuel jets: effects of ambient temperature, ambient density, and injection pressure. Combustion and Flame, Volume 138, Issues 1-2, July 2004, Pages 114–135, doi:10.1016/j.combustflame.2004.04.006.

[12] Dec JE. A conceptual model of DI diesel combustion based on laser-sheet imaging. SAE Paper 970873, 1997, doi: 10.4271/970873.

[13] Tree, D.R, Svensson, K. I. Soot processes in compression ignition engines. Progress in Energy and Combustion Science, Volume 33, Issue 3, June 2007, Pages 272–309, doi:10.1016/j.pecs.2006.03.002.

[14] López J., Martín J., García A., Villalta D., Warey A. Implementation of two color method to investigate late cycle soot oxidation process in a CI engine under low load conditions. Applied Thermal Engineering, Volume 113, 25 February 2017, Pages 878-890, doi: 10.1016/j.applthermaleng.2016.11.095.

[15] Benajes, J., Martin, J., Garcia, A., Villalta, D.,Warey A. et al. An Investigation of Radiation Heat Transfer in a Light-Duty Diesel Engine. SAE Int. J. Engines, Volume 8, Issue 5, 2015, doi:10.4271/2015-24-2443.

[16] Gallo, Y., Li, Z., Richter, M., and Andersson, O. Parameters Influencing Soot Oxidation Rates in an Optical Diesel Engine. SAE Int. J. Engines, Volume 9, Issue 4, 2016, doi:10.4271/2016-01-2183.

[17] Dembinski H., Angstrom H. Swirl and Injection Impact on After-Oxidation in Diesel Combustion, Examined with Simultaneous Combustion Image Velocimetry and Two Colour Optical Method. SAE Technical Paper 2013-01-0913, 2013, doi:10.4271/2013-01-0913.

[18] O'Connor J., Musculus M. Posts Injections for Soot Reduction in Diesel Engines: A Review of Current Understanding. SAE Int. J. Engines, Volume 6, Issue 1, 2013, doi:10.4271/2013-01-0917.

[19] Arrègle J., Pastor J.V., López J., García A. Insights on postinjection-associated soot emissions in direct injection diesel engines. Combustion and Flame, Volume 154, August 2008, Pages 448-461. doi: 10.1016/j.combustflame.2008.04.021.

[20] Lopez J., Martin J., Garcia A., Villalta D. et al. Characterization of In-Cylinder Soot Oxidation Using Two-Color Pyrometry in a Production Light-Duty Diesel Engine. SAE Technical Paper 2016-01-0735, 2016, doi:10.4271/2016-01-0735.

[21] AVL manufacturer manual. Smoke value measurement with the filter-paper-method. Application notes. June 2005 AT1007E, Rev. 02. Web: https://www.avl.com/documents/10138/885893/Application+Notes.

[22] DRIVVEN Stand Alone Direct Injector Driver System User's Manual October 2010. Drivven, INC. 12001 Network Blvd, 110. San Antonio, Texas 78249. Web: www.drivven.com<http://www.drivven.com>

[23] Payri, F., Olmeda, P., Martin, J., and Carreño, R. A New Tool to Perform Global Energy Balances in DI Diesel Engines. SAE Int. J. Engines, Volume 7, Issue 1, 2014, doi:10.4271/2014-01-0665.

[24] Zhao H., Ladommatos N. Optical diagnostics for soot and temperature measurement in diesel engines. Progress in Energy and Combustion Science, Volume 24, no. 3, Pages 221-255, doi:10.1016/S0360-1285(97)00033-6.

[25] Benajes, J., Olmeda, P., Martín, J. and Carreño, R. A new methodology for uncertainties characterization in combustion diagnosis and thermodynamic modelling. Applied Thermal Engineering, Volume 71, 5 October 2017, Pages 389-399, doi:10.1016/j.applthermaleng.2014.07.010.

[26] Lapuerta M, Armas O, Hernández JJ. Diagnosis of DI Diesel combustion from in-cylinder pressure signal by estimation of mean thermodynamic properties of the gas. Applied Thermal Engineering, Volume 19, May 1999, Pages 513-29. doi.org/10.1016/S1359-4311(98)00075-1.

[27] Arrègle J., López J.J., García J.M., Fenollosa C. Development of a Zero Dimensional Diesel Combustion Model. Part 1: Analysis of the Quasi-steady Diffusion Combustion Phase. Applied Thermal Engineering, Volume 23, August 2003, Pages 1301-1317, doi:10.1016/S1359-4311(03)00079-6.

[28] Li X., Qiao Z., Su L., Liu F. The combustion and emission characteristics of a multi-swirl combustion system in a DI diesel engine. Applied Thermal Engineering, Volume 115, 25 March 2017, Pages 1203-1212, doi.org/10.1016/j.applthermaleng.2016.10.028.

[29] De la Morena J., Vassallo A. Peterson R.C., Gopalakrishan V., Gao J. Influence of Swirl Ratio on Combustion System Performance of a 0.4l Single-Cylinder Diesel Engine. THIESEL 2014 Conference on Thermo- and Fluid Dynamic Processes in Direct Injection Engines.

[30] Molina S., Desantes J., García A., pastor J. A Numerical Investigation on Combustion Characteristic with the use of Post Injection in DI Diesel Engines. SAE Techincal Paper 2010-01-1260,2010, doi:10.4271/2010-01-1260.

[31] Bobba M., Musculus M., Neel W. Effect of Post Injections on In-Cylinder and Exhaust Soot for Low-Temperature Combustion in a Heavy-Duty Diesel Engines. SAE Int. J. Engines, Volume 3, Issue 1, 2010, doi: 10.4271/2010-01-0612.

[32] Hocine A., Desmet B., Guenoun S. Numerical study of the influence of diesel post injection and exhaust gas expansion on the thermal cycle of an automobile engine. Applied Thermal Engineering Volume 30, October 2010, Pages 1889–1895. doi.org/10.1016/j.applthermaleng.2010.03.033.

Abbreviations

ACT: Apparent Combustion Time

BMEP: Brake Mean Effective Pressure

CA50: Crank Angle at 50% mass fraction burned

CAD: Crank Angle Degree

CI: Combustion Ignition

DI: Direct-Injection

EGR: Exhaust Gases Recirculation

EoC: End of Combustion

EoI: End of Injection

ET: Energizing Time

EVO: Exhaust Valve Open

FSN: Filter Smoke Number

FWHM: Full Width al Half Maximun

GHG: Greenhouse Gases

GIE: Gross Indicated Efficiency

ICE: Internal Combustion Engines

IVC: Inlet Valve Close

$I_{b,\lambda}$: Spectral Intensity of Black Body

I_{soot}: Spectral Intensity

KL: Optical Thickness

LOL: Lift-off Length

NOx: Nitrogen Oxides

P_{in}: Intake Pressure

PM: Particulate Matter

POC: Point of Combustion

POI: Point of Injection

RoHR: Rate of Heat Release

SoE: Start of Energizing

SR: Swirl Ratio

TDC: Top Dead Center

T_{in}: Intake Temperature

α: Absorptivity

ε: Emissivity

λ: Wavelength